Mon. Not. R. Astron. Soc. **000**, 1–6 (2013) Printed 7 August 2013 (MN LATEX style file v2.2)

A submillimetre-bright z $\sim$ 3 overdensity behind a z $\sim$ 1 supercluster revealed by SCUBA–2 and *Herschel**

A. G. Noble[1]†, J. E. Geach[1,2], A. J. van Engelen[3], T. M. A. Webb[1], K. E. K. Coppin[1,2], A. Delahaye[1], D. G. Gilbank[4], M. D. Gladders[5], R. J. Ivison[6,7], Y. Omori[1], H. K. C. Yee[8]

[1]*Department of Physics, McGill University, 3600 Rue University, Montréal, Québec, H3A 2T8, Canada*
[2]*Centre for Astrophysics Research, Science & Technology Research Institute, University of Hertfordshire, Hatfield, AL10 9AB*
[3]*Department of Physics and Astronomy, Stony Brook University, Stony Brook, NY, 11794-3800, USA*
[4]*South African Astronomical Observatory, PO Box 9, Observatory, 7935, South Africa*
[5]*Department of Astronomy and Astrophysics, University of Chicago, 5640 S. Ellis Ave., Chicago, IL, 60637, USA*
[6]*UK Astronomy Technology Centre, Science and Technology Facilities Council, Royal Observatory, Blackford Hill Edinburgh, EH9 3HJ, UK*
[7]*Institute for Astronomy, University of Edinburgh, Blackford Hill Edinburgh, EH9 3HJ, UK*
[8]*Department of Astronomy and Astrophysics, University of Toronto, 50 St George Street, Toronto, Ontario M5S 3H4, Canada*

ABSTRACT

We present a wide-field (30′ diameter) 850μm SCUBA-2 map of the spectacular three-component merging supercluster, RCS 231953+00, at $z = 0.9$. The brightest submillimetre galaxy (SMG) in the field ($S_{850} \approx 12$ mJy) is within 30″ of one of the cluster cores (RCS 2319–C), and is likely to be a more distant, lensed galaxy. Interestingly, the wider field around RCS 2319-C reveals a local overdensity of SMGs, exceeding the average source density by a factor of 4.5, with a $< 1\%$ chance of being found in a random field. Utilizing *Herschel*-SPIRE observations, we find three of these SMGs have similar submillimetre colours. We fit their observed 250–850μm spectral energy distributions to estimate their redshift, yielding $2.5 < z < 3.5$, and calculate prodigious star formation rates (SFRs) ranging from $500 - 2500\,\mathrm{M}_\odot\,\mathrm{yr}^{-1}$. We speculate that these galaxies are either lensed SMGs, or signpost a physical structure at $z \approx 3$: a 'protocluster' inhabited by young galaxies in a rapid phase of growth, destined to form the core of a massive galaxy cluster by $z = 0$.

Key words: galaxies: clusters: individual (RCS 231946+0030.6) – galaxies: formation – galaxies: evolution – galaxies: high-redshift – submillimetre: galaxies

1 INTRODUCTION

Submillimetre (submm) surveys have a history of exciting revelations, beginning with the discovery of a population of submm-bright galaxies (SMGs) over a decade ago (Smail et al. 1997; Barger et al. 1998; Hughes et al. 1998). These SMGs are now known to be high-z (Chapman et al. 2005; Wardlow et al. 2011), gas-rich (Frayer et al. 1998, 1999) systems undergoing intense episodes of star formation, and are the likely progenitors of massive elliptical galaxies seen locally (Eales et al. 1999; Lilly et al. 1999). The latest generation of submm telescopes, namely the *Herschel Space Observatory* (Pilbratt et al. 2010) and SCUBA-2 (Holland et al. 2013) on the James Clerk Maxwell Telescope (JCMT), are ushering in a new era of submm astronomy, yielding samples of thousands of SMGs (Eales et al. 2010; Oliver et al. 2012) and promising many discoveries (Chen et al. 2013; Geach et al. 2013; Casey et al. 2013).

The wide-field mapping power of SCUBA-2 opens up a new parameter space in submm studies: the capability to survey volumes that sample the full range of galaxy environment at high redshifts. The densest regions—the nodes in the cosmic web—at all epochs are rare. However, it is essential to understand the evolution of galaxies within these environments if we are to link the growth of galaxies with the large scale structure they inhabit. Submm studies of distant 'protoclusters' are particularly promising since it is becoming clear that the massive tail of the galaxy cluster 'red-sequence' assembles quickly at $z > 2$ (Papovich et al. 2010), possibly via intense starbursts within gas-rich galaxies located in overdense (but potentially pre-virialised) structures at high-z (Daddi et al. 2009). This activity might well be heavily dust-obscured, requiring submm and/or infrared (IR) observations to detect.

Here, we report early findings from a wide-field SCUBA-2 and *Herschel*-SPIRE survey of a spectacular merging $z = 0.9$ supercluster, RCS 231953+00 (hereafter RCS 2319+00;

* Herschel is an ESA space observatory with science instruments provided by European-led Principal Investigator consortia with important participation from NASA.

† E-mail: nobleal@physics.mcgill.ca

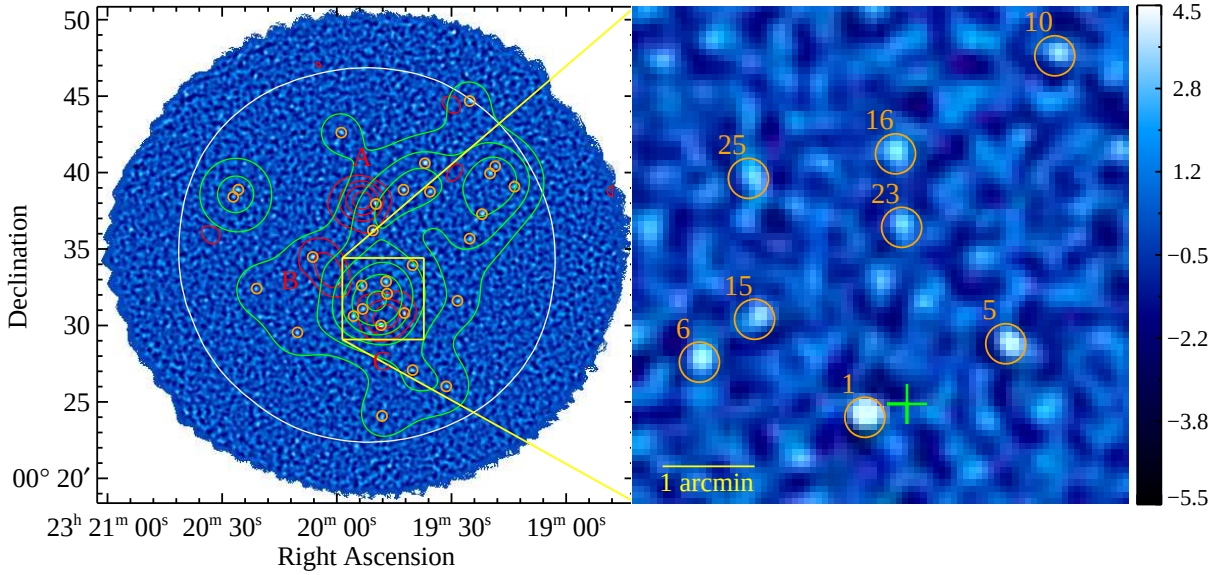

Figure 1. Left: 850μm signal-to-noise ratio map of the RCS 2319+00 supercluster overlaid with the red-sequence contours indicating the cluster positions in red. We highlight all SMGs detected at $>3.5\sigma$ in the 850μm map with orange circles. The green contours show the fractional overdensity of SMGs compared to the average density over the field, starting at $\delta = -0.3$ and increasing by levels of 0.7. The white circle represents the region from which sources are extracted. Right: a zoom-in on the overdensity of SMGs surrounding RCS 2319–C, labeled with their ID in the 850μm catalog. Given its proximity to the centre of RCS 2319–C (the BCG is marked by the green cross), the brightest source in the catalog, SMM J2319.1, is possibly lensed by the cluster potential.

Faloon et al. 2013). The structure comprises three massive ($\sim 5\times10^{14}$M$_\odot$), X-ray bright galaxy clusters (Hicks et al. 2008), namely RCS 231953+0038.1, RCS 232003+0033.5, and RCS 231946+0030.6 (hereafter RCS 2319–A, RCS 2319–B, and RCS 2319–C). The three clusters are separated by less than 3 projected Mpc and are expected to merge to form a single Coma-mass cluster by $z \sim 0.5$ (Gilbank et al. 2008). RCS 2319–A is a known strong-lensing cluster (Gladders et al. 2003), and the three cores appear to be connected by filamentary structure and satellite groups. The wealth of data and discoveries surrounding RCS 2319–A is extensive; RCS 2319–C, on the other hand, has thus far been comparatively inconspicuous due to a lack of wide-field coverage encompassing the entire structure.

RCS 2319+00 affords a unique opportunity to study the physics of galaxy formation across the full range of galaxy environments at $z \approx 1$, as well as more distant galaxies lensed by the cluster potential. In this Letter, we present a serendipitous discovery of an overdensity of SMGs behind RCS 2319–C, as well as a bright SMG close to the cluster core. This overdensity could result from a large number of lensed SMGs behind the cluster or represent a possible distant protocluster. This discovery along the line-of-sight to the RCS 2319 supercluster is a fortunate coincidence: it allows us to investigate the properties of SMGs within the densest environments in the Universe at two epochs within the same field, with the benefit that the more distant structure might be partially lensed by the supercluster. We assume a ΛCDM cosmology with $(\Omega_m, \Omega_\Lambda, h) = (0.3, 0.7, 0.7)$.

2 OBSERVATIONS AND DATA REDUCTION

2.1 The RCS 2319+00 Supercluster

Originally discovered in the Red-sequence Cluster Survey (RCS-1; Gladders & Yee 2005) and presented in Gilbank et al. (2008), the RCS 2319+00 structure now has extensive follow-up observations. Much of the work has focused on the northern-most cluster (RCS 2319–A); it was revealed to be a remarkable strong-lensing cluster with three gravitationally lensed radial arcs (Gladders et al. 2003), and has a significant weak lensing signal (Jee et al. 2011). SCUBA imaging of the core of RCS 2319–A unveiled a candidate lensed SMG (Noble et al. 2012) and *Herschel*-SPIRE imaging revealed a 2.5 Mpc filament of SMGs connecting RCS 2319–A to its eastern companion, RCS 2319–B (Coppin et al. 2012).

2.2 850μm SCUBA–2 observations

SCUBA-2 observations were conducted at the JCMT in Band 2 weather ($0.05 < \tau_{225\,\mathrm{GHz}} < 0.08$) between 17–21 September 2012 using the 30′ PONG mapping pattern. The total mapping time was 7.75 hr, split into 11× 40 min scans. Individual scans are reduced using the dynamic iterative map-maker (*makemap*) of the SMURF package (Chapin et al. 2013) following the procedure outlined in Geach et al. (2013). These scans are co-added in an optimal, noise-weighted manner, using the `MOSAIC_JCMT_IMAGES` recipe in the PICARD environment. Finally, to improve the detectability of faint point sources, we use `SCUBA2_MATCHED_FILTER`, which removes large angular scale varying pattern noise in the map by smoothing with a 30” Gaussian kernel, subtracting this, and then convolving the map with the 850μm beam. The average exposure time over the ‘nominal’ 30′ mapping region in the co-added map is ≈10 ksec, reaching a central depth of 1.5 mJy.

2.3 *Herschel*-SPIRE observations

The *Herschel*-SPIRE (Griffin et al. 2010) data were taken on January 2, 2013, with a total of 8.1 hours of integration time over five dithered maps at 250, 350, and 500μm (OBSIDs 1342258348,

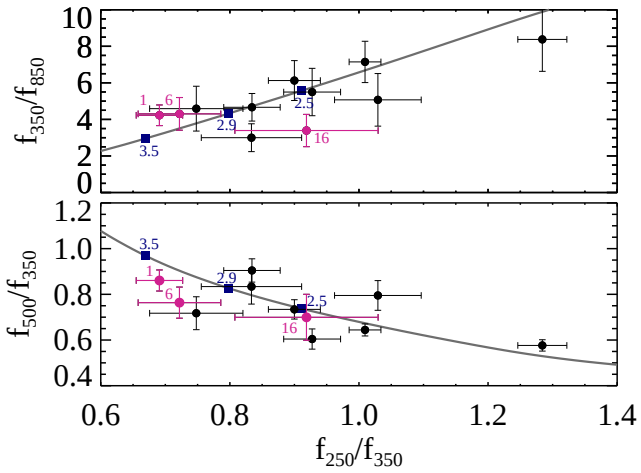

Figure 2. Submm/far-IR colour ratios for all SMGs that have unblended SPIRE counterpart emission in the top panel, and solely SPIRE colors in the bottom panel. Both plots show the change of these colour ratios (gray line) with redshift using the median luminosity template from Chary & Elbaz (2001), where the navy squares denote $z = 2.5, 2.9, 3.5$. The possible protocluster members are highlighted in pink, and are at the higher-z end of the distribution with similar far-IR/submm colours. Confusion errors are not shown for clarity.

1342258349, 1342258350, 1342258351, 1342258352). The observations cover $30' \times 30'$, including all three cluster cores, and were carried out in array mode using the nominal scan speed. Each map is reprocessed individually using HIPE V10.0 (Ott 2010) and the latest calibration tree. One map has significant artifacts and requires a linear polynomial fit during the destriping process; all other maps are destriped using a zeroth-order fit. All Level 1 scans are merged and final mosaiced images created using the naïve mapper with default pixel sizes of $6''$, $10''$, and $14''$, at 250, 350, and 500μm, respectively.

Point sources are extracted using SUSSEXtractor (Savage & Oliver 2007) at a relatively low detection threshold of 3.5σ to maximize counterpart completeness. The source list is passed to a timeline fitter that utilizes the merged Level 1 timeline data to fit a Gaussian at the source position. For sources below 30 mJy, the flux is measured as the peak on the image after smoothing with a convolution kernel and using a sub-pixel correction factor. This has been found to be a more reliable flux estimate for faint sources (SPIRE Webinar, private communication). The uncertainties on the fluxes are estimated from pixel noise added in quadrature with a nominal confusion noise of 5.8, 6.3, and 6.8 mJy at 250, 350, and 500μm, respectively (Nguyen et al. 2010).

3 ANALYSIS AND RESULTS

Point sources are extracted from the central $\sim 25'$ of the beam-convolved map, where the sensitivity is fairly uniform and the noise is $< 3\times$ the central 1σ r.m.s., corresponding to a total uniform area of $\sim$473 arcmin^2. We detect 29 point sources at 850μm at a significance of $>3.5\sigma$, 16 of which are at $> 4\sigma$. The detections are indicated by orange circles in Figure 1 and named in order of descending signal-to-noise ratio. We quantify the false-detection rate by running the detection algorithm on jack-knife versions of the map (details given in Geach et al. 2013). Within the source detection area, we find a false-detection rate of 4.5% (20%) at 4.0σ (3.5σ). We note that both these rates are 25% lower where the noise is $< 2\times$ the central r.m.s., encompassing all but one of the SMGs.

3.1 SCUBA–2/SPIRE source identification

Very Large Array radio imaging at 1.4 GHz covers the entirety of the SCUBA-2 and SPIRE maps, although with roughly $2\times$ the noise at the edges due to primary beam attenuation (Noble et al. 2012). We also exploit deep IR imaging from the Multiband Imaging Photometer (MIPS) aboard *Spitzer* (Webb et al. 2013). The extensive, multi-wavelength counterpart identification process, including the completeness and false-detection rate, will be presented in Noble et al. (in preparation); we provide only a brief description in this communication.

Given the $\approx 15''$ beam at 850μm, we search for radio and 24μm emission within $10''$ of the SCUBA-2 positions, ensuring we detect all possible counterparts (Ivison et al. 2007; Biggs et al. 2011). While a $10''$ search radius is generous, in practice we find that all the counterparts to $>4\sigma$ SMGs are within $6''$, with an average offset of $3''$. We robustly detect a 24μm and/or radio counterpart for 20 of the 29 (70%) sources within our catalog. Of the remaining SCUBA-2 detections, eight lack MIPS coverage (and have no radio detection), and one source eludes any counterpart emission. For cases where multiple 24μm sources are detected within the search area (and no radio emission), we assign the nearest source as the most likely counterpart, which in all occurrences is also the brightest 24μm detection within the search area.

Counterpart SPIRE emission can further verify the validity of each SCUBA-2 source, although it is not a requirement as 20–60% of $z > 2$ SMGs are undetectable with SPIRE (Casey et al. 2012). Given the large SPIRE beam, we search within the entire SCUBA-2 beam for 250–500μm emission, resulting in detections in one or more SPIRE bands for 18 of the 29 850μm sources. Four of the SMGs lacking MIPS coverage or a radio counterpart are detected with SPIRE, yielding a final catalog of 24 (80%) SCUBA-2 sources with counterparts in another band. Any emission that is blended or confused in SPIRE (four cases in total) is omitted from the counterpart catalog for the purposes of far-IR SED fitting (see §3.2).

3.2 Evidence of a line-of-sight, submillimetre-bright protocluster

The average surface density of 850μm sources across the $30'$ RCS 2319+00 field is consistent with that expected from the number counts measured in blank-field submm surveys (Coppin et al. 2006); however, it is clear that there are large variations in the local surface density on scales of several arcminutes. Indeed, there appears to be a local relative overdensity of 850μm detections in the vicinity of RCS 2319–C. To quantify this, we create a Gaussian smoothed ($\theta = 4'$) surface density map, normalized to the fractional overdensity of SMGs: $\delta_{\rm peak} = (\rho - \bar{\rho})/\bar{\rho}$ (Figure 1).

There is a $\delta_{\rm peak} = 3.5$ close to RCS 2319–C. To assess the significance of this local peak, we generate simulated catalogues of the same size as the real map, and with the same source density as the detected SMGs. In addition to the shot noise properties of the sources, we also include the effects of clustering on linear scales, assuming a redshift distribution and bias factor matching the current best estimate for 850μm-selected SMGs (Hickox et al. 2012). We check the clustering properties of the fake catalogues by applying the Landy-Szalay estimator (Landy & Szalay 1993) and find the angular correlation function $w(\theta)$ to be consistent with

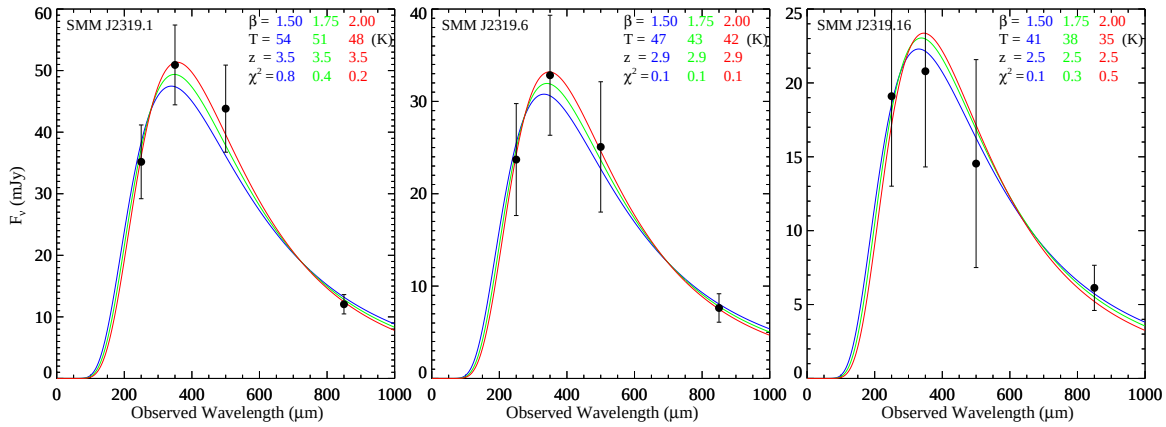

Figure 3. Modified blackbody fits to the SPIRE and SCUBA-2 fluxes for the three possible protocluster members, using the technique described in Section 3.2. The parameters for the best fit values with β fixed at 1.5 (blue), 1.75 (green) and 2.0 (red) are listed in each panel. The lowest reduced χ^2 values are given by $z = [3.5, 2.9, 2.5] \pm 0.6$ and $T_{\rm d} = [48, 43, 41] \pm 8$ K for SMMs J2319.1, 2319.6, and 2319.16, respectively. We note that SMM J2319.1 has only a weak radio detection, just below the catalogue limit; we therefore assign it the 3σ rms limit of 45μJy.

Hickox et al. (2012) at $\theta \gtrsim 1'$, matching the scale of the candidate protocluster. We generate 1000 catalogue realisations, each time evaluating the convolved surface density estimate, as described above. The total number of density peaks found with $\delta \geqslant \delta_{\rm peak}$ is an estimate of the significance of finding a local overdensity of magnitude 3.5 or greater in our map. We find nine such peaks over all 1000 realisations, meaning the SMG overdensity is very unlikely to be due to Poisson noise or clustering from large scale structure, significant at a level of 99%. In other words, such a structure is rare, even given the known correlation function of SMGs, and thus could point to the presence of a real physical association of SMGs tracing a highly biased structure.

With four submm bands, we can also compare the submm colours of the SMGs around RCS 2319–C to test if they have similar far-IR SEDs (and therefore possibly similar redshifts) in addition to a spatial correlation. In Figure 2, we plot the SPIRE and SCUBA-2 colours of 11 SMGs that are detected in all three SPIRE bands. We do not include 8 sources that have blended SPIRE emission. The sources within the overdensity are highlighted in pink, and lie at the higher redshift end of the colour distribution compared to the other SMGs in the field. SMM J2319.1 and SMM J2319.6 are quite distinct, while SMM J2319.16 tends towards the bluer end of the S_{250}/S_{350} distribution, but is still within $\sim$1σ of the other putative protocluster galaxies.

We estimate the redshifts of these sources by fitting to the submm photometry, assuming the SED can be modeled by a single temperature modified blackbody, with a smooth transition into a power law on the Wien side. Because of the degeneracy in the z–T–β parameter space, we perform three fits, each time only allowing z and T to be free parameters ($20 < T < 60$ K), while fixing β at 1.5, 1.75 and 2, spanning the likely range of real galaxies (Dunne et al. 2000). We further improve upon the estimate by putting prior constraints on z and T from independent measurements, as shown in Roseboom et al. (2012). We estimate a submm-radio photo-z using the spectral index relation from Carilli & Yun (1999), assuming $\alpha_{1.4{\rm GHz}} = -0.8$, $\alpha_{850\mu m} = \beta + 2$, and a typical uncertainty of $\Delta z = 1.0$ (Aretxaga et al. 2007). We also simultaneously measure the total (8–1000μm rest-frame) IR luminosity to estimate S_{60}/S_{100} using the empirical relation in Roseboom et al. (2012) from a SPIRE-selected sample. We then convert the flux ratio into a dust temperature from the modified blackbody described above and conservatively assume a 10 K scatter in T_d.

This fitting algorithm greatly reduces the degeneracy between z and T_d and produces typical uncertainties of $\Delta z = 0.6$ and $\Delta T_d = 8$ K. The best fit SEDs are shown in Figure 3. The lowest values of χ^2/ν yield z =[3.5, 2.9, 2.5] and T_d =[48, 43, 41] K for SMMs J2319.1, J2319.6, and 2319.16, respectively. These redshifts are all within $\sim 1\sigma$ and further support the existence of an SMG protocluster behind RCS2319-C at $z > 2.5$. Although this redshift range is representative of the typical SMG (Chapman et al. 2005), we emphasize the similarity of submm colours for these SMGs, which isolates them from the rest of the sample through a consistent comparison. The SED fit also provides an estimate of the IR luminosity which can be converted to a SFR (Salpeter IMF; Kennicutt 1998); we find all three candidate protocluster members are highly active, with SFRs of 2500, 1100, and 500 $\rm M_\odot\,yr^{-1}$(assuming no AGN contamination). We note that these could be over estimated if any of the SMGs are strongly lensed.

3.3 A submillimetre-bright, strongly lensed galaxy

Within this putative protocluster lies the brightest 850μm source in the catalogue, SMM J2319.1, with $S_{850} = 12.05 \pm 1.56$ mJy. This source is only 28″ away from the X-ray peak of RCS2319–C and could be strongly lensed by the cluster potential, though it is only 1.5× as bright as the second brightest protocluster member. SMM J2319.1 is coincident with an extremely red spur-like feature—possibly the optical/near-IR counterpart to the SMG. It is considerably redder than the red-sequence galaxies in the cluster, implying that it is probably at higher redshift. Indeed, the SED fit places this source at $z = 3.5$, although (sub)mm spectroscopic identification will be required to accurately determine the redshift.

In Figure 4 we present a *gK*[4.5] composite image of the cluster core. 850μm S/N contours mark the position of the galaxy. There are hints of a blue arc-like feature around the BCG, indicating that this may be a strong lensing cluster. We lack an accurate mass model for this cluster (high-resolution optical imaging only exists for RCS 2319–A), but assuming an isothermal sphere with $\sigma_v = 759\,{\rm km\,s^{-1}}$ (Faloon et al. 2013) and $z = 3.0$ for the source plane, we calculate an Einstein radius of $\sim 9''$, which is consistent

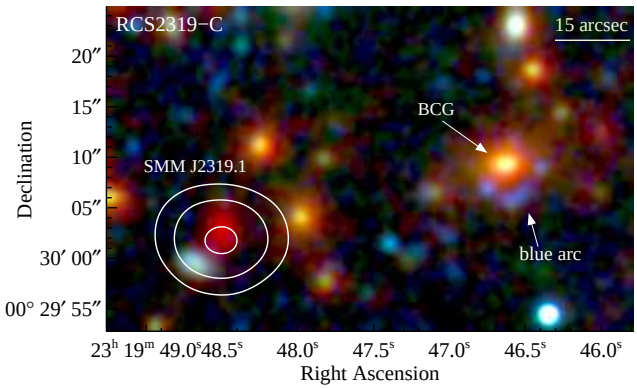

Figure 4. A *gK*[4.5] colour composite (from CFHT and IRAC) of the centre of RCS 2319–C, showing the position of with SMM J2319.1, the possible lensed SMG (850μm S/N contours starting at 5σ, increasing by levels of 1σ), Note the very red optical/near-IR emission coincident with the SCUBA-2 detection. We highlight the BCG, with a blue arc-like feature to the south, further indicating that this could be a strong-lensing cluster.

with the distance between the BCG and blue arc. We emphasize that the projected overdensity of SMGs around RCS2319–C could also be due to boosted counts from lensing of the random field, rather than a physical protocluster (spectroscopic confirmation will answer this question). However, the peak of the overdensity is offset from the core of RCS 2319–C by $>1'$, while the average lensing magnification beyond the central $30''$ is expected to be < 2 for similarly massive clusters (Noble et al. 2012).

4 SUMMARY

This Letter presents the first wide-field SCUBA-2 850μm map of a high-z galaxy cluster field. We target a rare, three-component supercluster at $z = 0.9$ – RCS 2319+00 – detecting 29 SMGs, the majority of which have robust counterparts at 24μm, 1.4 GHz and/or in the *Herschel*-SPIRE bands. Previous work on RCS 2319+00 has focused on the northern core, RCS 2319–A, which is a well-known strong-lensing system, whereas the new SCUBA–2 map reveals that RCS2319–C, the southern-most component, also has some interesting traits. We make two discoveries:

(i) RCS2319–C has features indicative of a strongly lensing cluster, with a distinct blue arc just below the BCG (at a radius consistent with the Einstein radius expected for this cluster). We report the discovery of a bright ($S_{850} \approx 12$ mJy) SMG $28''$ from the core, associated with a very red optical/near-IR counterpart that is likely to be a lensed galaxy at $z \approx 3$. Thus, it offers the rare opportunity to study the properties of the SMG in much finer detail than would otherwise be possible.

(ii) There is a significant local overdensity of SMGs in the vicinity of RCS2319–C, with a peak of $\delta = 3.5$ in density contrast when smoothed at $4'$. Simulations indicate that there is a <1% chance of finding a similar structure in a (clustered) blank field of the same area. We estimate the redshifts for three of the sources within this overdensity by fitting the observed 250–850μm photometry with a modified blackbody SED, finding them consistent with $2.5 < z < 3.5$. They have high IR luminosities, corresponding to SFRs ranging from $500 - 2500\,\mathrm{M}_\odot\,\mathrm{yr}^{-1}$. We speculate that the SMGs are part of a physical association at $z \approx 3$, perhaps signposting a starbursting protocluster along the line of sight to RCS 2319–C. This scenario is supported by recent clustering measurements which predict the formation of SMGs in compact protoclusters (Maddox et al. 2010). Indeed, SMGs have been found to trace the underlying distribution of Lyman-α emitters in a $z \approx 3.1$ protocluster (Tamura et al. 2009) and in some cases are physically associated with Lyα Blobs in these enviroments (Chapman et al. 2001; Geach et al. 2005).

We thank many people for assistance with the SCUBA-2/SPIRE data, including the JAC staff and telescope operators, and the SPIRE ICC, especially David Shupe. We also thank Gaelen Marsden for useful discussions. JG acknowledges support from a Banting Fellowship administered by NSERC. TW is supported by the NSERC Discovery Grant and the FQRNT Nouveaux Chercheurs program. KC receives support from the endowment of the Lorne Trottier Chair in Astrophysics and Cosmology at McGill and NSERC.

REFERENCES

Aretxaga, I., et al. 2007, MNRAS, 379, 1571
Barger, A. J., Cowie, L. L., Sanders, D. B., Fulton, E., Taniguchi, Y., Sato, Y., Kawara, K., & Okuda, H. 1998, Nature, 394, 248
Biggs, A. D., et al. 2011, MNRAS, 413, 2314
Carilli, C. L., & Yun, M. S. 1999, ApJ, 513, L13
Casey, C. M., et al. 2012, ApJ, 761, 140
—. 2013, ArXiv e-prints
Chapin, E. L., Berry, D. S., Gibb, A. G., Jenness, T., Scott, D., Tilanus, R. P. J., Economou, F., & Holland, W. S. 2013, MNRAS, 430, 2545
Chapman, S. C., Blain, A. W., Smail, I., & Ivison, R. J. 2005, ApJ, 622, 772
Chapman, S. C., Lewis, G. F., Scott, D., Richards, E., Borys, C., Steidel, C. C., Adelberger, K. L., & Shapley, A. E. 2001, ApJ, 548, L17
Chary, R., & Elbaz, D. 2001, ApJ, 556, 562
Chen, C.-C., Cowie, L. L., Barger, A. J., Casey, C. M., Lee, N., Sanders, D. B., Wang, W.-H., & Williams, J. 2013, ApJ, 762, 81
Coppin, K., et al. 2006, MNRAS, 372, 1621
Coppin, K. E. K., et al. 2012, ApJ, 749, L43
Daddi, E., et al. 2009, ApJ, 694, 1517
Dunne, L., Eales, S., Edmunds, M., Ivison, R., Alexander, P., & Clements, D. L. 2000, MNRAS, 315, 115
Eales, S., Lilly, S., Gear, W., Dunne, L., Bond, J. R., Hammer, F., Le Fèvre, O., & Crampton, D. 1999, ApJ, 515, 518
Eales, S., et al. 2010, PASP, 122, 499
Faloon, A. J., et al. 2013, ApJ, 768, 104
Frayer, D. T., Ivison, R. J., Scoville, N. Z., Yun, M., Evans, A. S., Smail, I., Blain, A. W., & Kneib, J.-P. 1998, ApJ, 506, L7
Frayer, D. T., et al. 1999, ApJ, 514, L13
Geach, J. E., et al. 2005, MNRAS, 363, 1398
—. 2013, MNRAS, 432, 53
Gilbank, D. G., Yee, H. K. C., Ellingson, E., Hicks, A. K., Gladders, M. D., Barrientos, L. F., & Keeney, B. 2008, ApJ, 677, L89
Gladders, M. D., Hoekstra, H., Yee, H. K. C., Hall, P. B., & Barrientos, L. F. 2003, ApJ, 593, 48
Gladders, M. D., & Yee, H. K. C. 2005, ApJS, 157, 1
Griffin, M. J., et al. 2010, A&A, 518, L3
Hickox, R. C., et al. 2012, MNRAS, 421, 284
Hicks, A. K., et al. 2008, ApJ, 680, 1022

Holland, W. S., et al. 2013, MNRAS, 430, 2513
Hughes, D. H., et al. 1998, Nature, 394, 241
Ivison, R. J., et al. 2007, MNRAS, 380, 199
Jee, M. J., et al. 2011, ApJ, 737, 59
Kennicutt, Jr., R. C. 1998, ARA&A, 36, 189
Landy, S. D., & Szalay, A. S. 1993, ApJ, 412, 64
Lilly, S. J., Eales, S. A., Gear, W. K. P., Hammer, F., Le Fèvre, O., Crampton, D., Bond, J. R., & Dunne, L. 1999, ApJ, 518, 641
Maddox, S. J., et al. 2010, A&A, 518, L11
Nguyen, H. T., et al. 2010, A&A, 518, L5
Noble, A. G., et al. 2012, MNRAS, 419, 1983
Oliver, S. J., et al. 2012, MNRAS, 424, 1614
Ott, S. 2010, in ASPCS, Vol. 434, Astronomical Data Analysis Software and Systems XIX, 139
Papovich, C., et al. 2010, ApJ, 716, 1503
Pilbratt, G. L., et al. 2010, A&A, 518, L1
Roseboom, I. G., et al. 2012, MNRAS, 419, 2758
Savage, R. S., & Oliver, S. 2007, ApJ, 661, 1339
Smail, I., Ivison, R. J., & Blain, A. W. 1997, ApJ, 490, L5+
Tamura, Y., et al. 2009, Nature, 459, 61
Wardlow, J. L., et al. 2011, MNRAS, 415, 1479
Webb, T., et al. 2013, ArXiv e-prints